Hindawi Publishing Corporation
International Journal of Distributed Sensor Networks
Volume 2012, Article ID 409048, 7 pages
doi:10.1155/2012/409048

Research Article

Real-Time Train Wheel Condition Monitoring by Fiber Bragg Grating Sensors

Chuliang Wei,[1] Qin Xin,[2] W. H. Chung,[3] Shun-yee Liu,[3] Hwa-yaw Tam,[3] and S. L. Ho[3]

[1] *Department of Electronic Engineering, Shantou University, Guangdong 515063, China*
[2] *Department of Applied Mathematics, Université catholique de Louvain 1348, Louvain-la-Neuve, Belgium*
[3] *Department of Electrical Engineering, The Hong Kong Polytechnic University, Kowloon, Hong Kong*

Correspondence should be addressed to Qin Xin, xin@simula.no

Received 25 July 2011; Accepted 8 August 2011

Academic Editor: Tai Hoon Kim

Wheel defects on trains, such as flat wheels and out-of-roundness, inevitably jeopardize the safety of railway operations. Regular visual inspection and checking by experienced workers are the commonly adopted practice to identify wheel defects. However, the defects may not be spotted in time. Therefore, an automatic, remote-sensing, reliable, and accurate monitoring system for wheel condition is always desirable. The paper describes a real-time system to monitor wheel defects based on fiber Bragg grating sensors. Track strain response upon wheel-rail interaction is measured and processed to generate a condition index which directly reflects the wheel condition. This approach is verified by extensive field test, and the preliminary results show that this electromagnetic-immune system provides an effective alternative for wheel defects detection. The system significantly increases the efficiency of maintenance management and reduces the cost for defects detection, and more importantly, avoids derailment timely.

1. Introduction

Condition monitoring measures are crucial to ensure safe and cost-effective train operation in the railroad transportation industry. A well-designed monitoring system substantially reduces hardware maintenance cost and improves service quality and overall safety. Wheel condition monitoring is one of the critical features in railway condition monitoring system. Typical train wheel defects include flat wheels, out-of-roundness (OOR), spalling, and shelling [1–3]. If wheel defects are not detected and rectified in time, the wheel may deteriorate rapidly and induce more frictional force that inflicts further defect on both wheels and rails.

Nowadays, railway operators usually detect wheel defects by visual checking with experienced workers on a regular basis. Passenger complaint or driver report of excessive vibration is another means of identifying wheel defects. Moreover, periodical scheduled wheel reprofiling according to engineering experiences without defects identification is also employed. These methods are useful in general but they do not guarantee in-time identification of wheel defects. The railway operators have to bear the high cost for regular wheel-checking and reprofiling, and the comfort of passengers is adversely affected due to high vibration. Worst still, there is always a higher risk of derailment. Thus, a real-time monitoring system which is reliable, safety-proven, and cost-effective for handling wheel defects problem is urgently required.

Many studies have been carried out to realize wheel defect detection and most of them are based on the analysis of wheel-rail interaction [2–6]. Attivissimo et al. used a laser diode and a CCD camera to measure wheel and rail head profiles and hence to evaluate the wheel-rail interaction quality [2]. The system is able to discover anomalies of wheel-rail contact, but not resolving the defects of wheel or rail. In addition, the laser source and camera require precision setup which is difficult for practical railroad application. To study possible causes and effects of OOR wheels, strain gauges and accelerometers were employed to measure the vertical wheel-rail contacting force and track response [3, 4], a number of 99 selected wheels were tested over a 100,000 km traveling distance. Since the sensitivity of the system is relatively low, only the wheels with local defects of 0.5 m in length can be identified. Sensors based

on ultrasonic [5] and acoustic [7] techniques have also been employed to measure the wheel and rail conditions, but the performance of these sensors are easily compromised under electromagnetic interference (EMI) railroad environment. Besides, EMI free fiber optics sensor [8] has been used to study the wheel defect problem, speckle interferometry in multimode optical fiber was developed to detect flat wheels of train. However, other types of defects such as local spall or polygonal wheel cannot be retrieved.

In this paper, we propose a real-time wheel-defect detection system based on fiber Bragg grating (FBG) sensors. The sensors measure the rail strain response upon wheel-rail interaction and the frequency component that solely reveals the quality of the interaction are extracted from the signal and processed in order to deduce the defects of passing wheels. One of the advantages of this sensor system is that both the sensors and connecting fibers installed at the railroad side are passive to EMI and they require no electric power until the head-end measurement equipment which could be tens of kilometers away from the measurement points. This feature is particularly favorable to the modern electrified railway system since the sensing network is immunized from EMI. In addition, the system allows in-service and real-time monitoring of wheel condition, which is attractive to the railway industry. Moreover, the system can also be integrated with other railroad FBG sensing applications [9–13] that have been reported previously.

The organization of this paper is as follows. The basic concept of FBG sensor and its characteristics are first reviewed, followed by the descriptions of the sensor packaging and field test; the measurement results and the algorithm to generate the condition index (CI) of wheel are presented; discussions and conclusions are also given at the subsequent sections.

2. FBG Sensor and Wavelength Interrogation System

FBG sensor is an in-fiber narrowband reflective optical filter resulted from periodical variation of refractive index inside the core of optical fiber. A conventional way to fabricate a FBG sensor is to illuminate a short section of optical fiber by ultraviolet laser source under a phase mask, the periodical pattern of the mask is photo-imprinted onto the optical fiber by modulating the refractive index of the fiber core. The Bragg wavelength λ_B of FBG sensor written in single-mode optical fiber is given below [14]:

$$\lambda_B = 2n\Lambda, \tag{1}$$

where n is the effective refractive index of the fiber core and Λ is the period of the refractive index modulation. Figures 1(a) and 1(b) illustrate an FBG sensor and its spectral characteristics. When a broadband light source is passed onto a sensor, a narrowband optical spectrum centered at λ_B is reflected while others pass through. Mechanical and thermal perturbations alter the modulation pitch as well as refractive index of the FBG and hence λ_B. By measuring the wavelength change of the FBG sensor, these perturbations can be determined. Typical wavelength changes of FBG written in standard single-mode fiber at 1550 nm region due to mechanical strain and temperature variation are ~1 pm/$\mu\varepsilon$ and ~11 pm/°C, respectively. Because of its compact size, low optical loss, self-referencing, and wavelength multiplexing capability, FBG sensors have been widely applied in a wide range of condition monitoring applications [9, 15–19].

An interrogator is employed to measure the wavelength of FBG sensor array. Figure 1(c) shows a simplified schematic of a typical FBG interrogator. To produce a wavelength tunable optical source with high output power for accurate wavelength measurement, scanning ring laser consists of an optical amplifier and a tunable narrowband Fabry-Perot filter in a ring cavity configuration is employed, the laser scans the FBG sensor array periodically and the signal reflected from the FBG sensors is directed to the photodetector through an optical circulator. The photodetector performs optical to electrical domain conversion, any peak in the converted electric signal reflects the existence of an FBG and the wavelength of the FBG can be retrieved by the timing of scanning signal. Commercially available interrogators usually have four measurement channels with a wavelength measuring range of ~80 nm, depending on the spectral occupancy of the FBG sensors in the array. Up to 40 serially connected FBG sensors (assuming 1 nm measuring range with 0.5 nm guard-band at both longer and shorter wavelength sides) can be measured simultaneously at a maximum sampling rate of 2 kHz by a single measurement channel. In this study, a four-channel interrogator with a sampling rate of 1 kHz is used.

3. Sensor Packaging and Field Test

Phase masks and ultraviolet excimer laser are used to fabricate the 10 mm-long FBG sensors in this study. To improve the photosensitivity of the standard single-mode fiber for FBG inscription, the fiber is kept in high pressure hydrogen vessel for a week. After FBG sensor fabrication, the fiber is annealed in temperature chamber and the FBG sensor section is recoated with the acrylate material. A 1 mm thickness stainless steel sheet with a dimension of 50 mm (length) and 12 mm (width) is machined using photochemical etching technique to form the sensor package as shown in Figure 2(a). This sensor package is designed in such a way that it allows a good mechanical contact between the FBG sensor and the rail surface while providing sufficient protection to the fiber. A 10 mm (length) and 8 mm (width) rectangular-shape void at the center of the package is used to place the FBG sensor during assembling, four elliptical recessed pads with a depth of 0.7 mm are used for electric spot-welding to the rail during on-site sensor installation. U-shape recessed grooves with a width and depth of 1 mm and 0.5 mm, respectively, are designed for fiber alignment and attachment purposes.

The sensor package is tested substantially by a calibration platform shown in Figure 2(b), a stainless steel triangular beam with one end fixed and the other end coupled to a mechanical joint which converts the rotational motion generated by a motor to a bending movement of the beam.

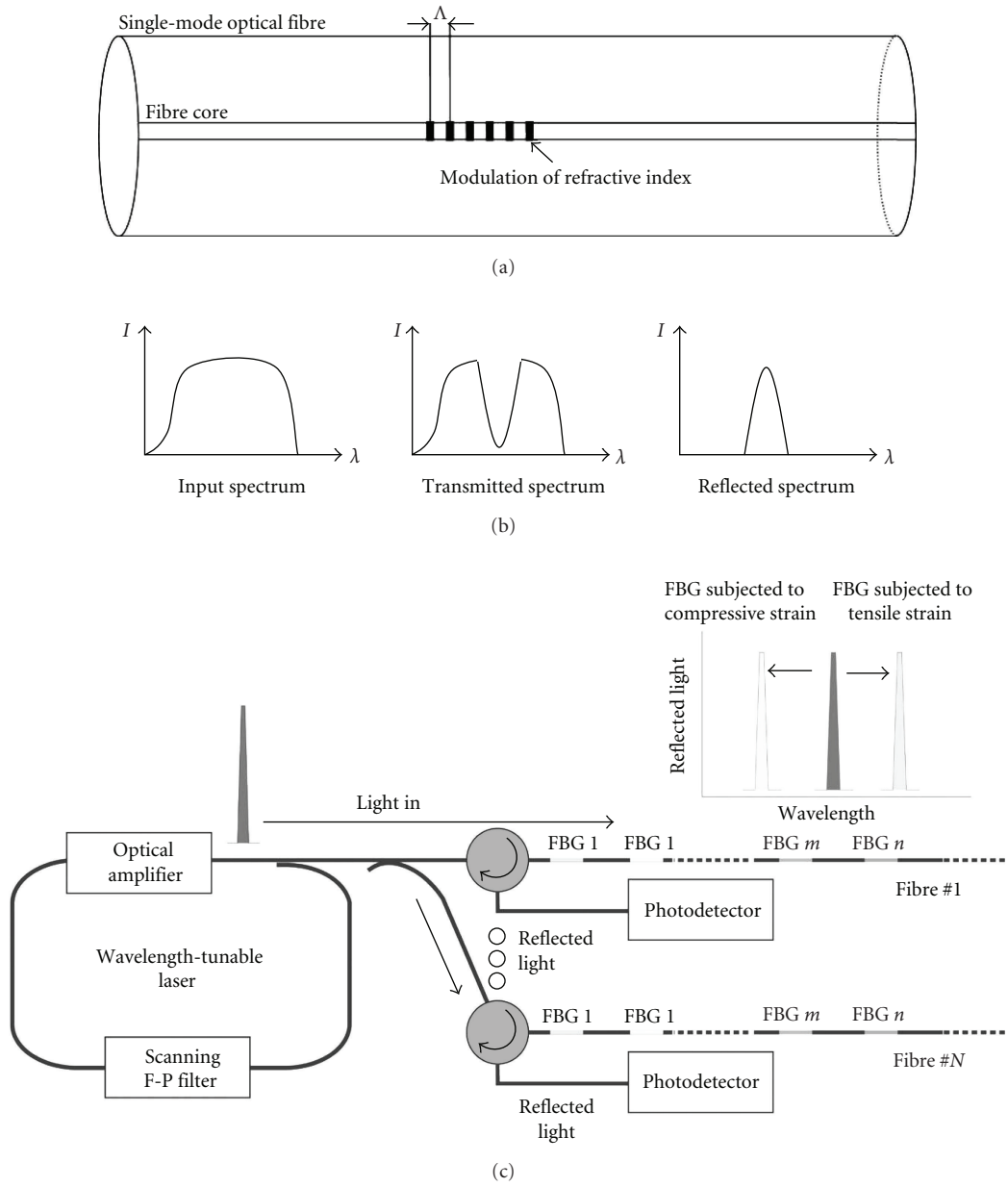

Figure 1: (a) Illustration of an FBG sensor; (b) the spectral response of FBG sensor; (c) block diagram of an FBG interrogator.

Strain gauges and the packaged FBG sensors are attached onto the beam for a back-to-back comparison. The motor, strain gauges reader, and the FBG interrogator are controlled by a computer for data logging. Performance and robustness of the packaged FBG sensors are maintained after thousands of bending cycles.

The field test has been performed in the East Rail line of the Hong Kong Mass Transit Railway (MTR). It is a heavily used suburban railway line with both passenger and freight services connecting Hong Kong urban districts to the border with mainland China. There are 14 intermediate stations and its length is over 30 km. The majority of track-form is the conventional ballast track with a maximum train speed of 130 km/h. Two independent pairs of tracks are used to provide traveling services for two opposite (i.e., north-bound and south-bound) directions.

Four sensors have been installed by spot-welding onto two pairs of rail tracks near the Ho Tung Lau (HTL) depot in the East Rail line. Train speed at the measurement point is 50 to 90 km/h with ballast track-form. The sensors are installed near the foot of the rail which is the most sensitive and practical position [13] for measuring the wheel-rail interaction. The rail has been slightly polished to provide a clean contact surface area for spot welding of the sensors. Arrangement of the sensor installation is shown in Figure 3, FBGs 1 and 2 are used to measure north-direction track; and FBGs 3 and 4 are for south-direction track. A pair of sensors (FBGs 1 and 2 or FBGs 3 and 4) is installed at the

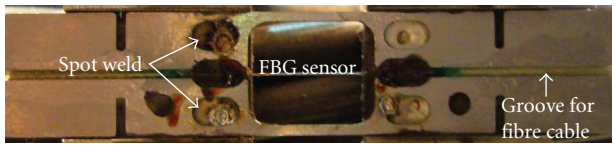

(a)

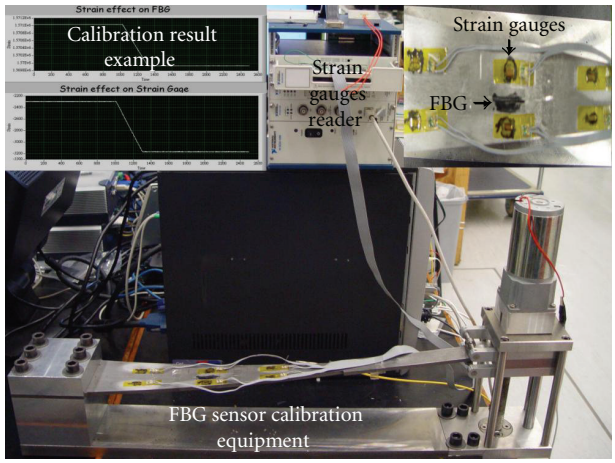

(b)

Figure 2: (a) Package of FBG sensor; (b) calibration platform in laboratory.

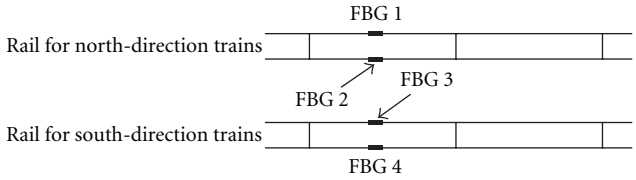

Figure 3: The FBG sensors installation scheme.

same location to ensure the two wheels of an axle passing the two measurement points at the same instant. The four sensors are connected in series as an array and linked to the interrogator through 2 km of outdoor optical cables. Real-time cameras and RFID receivers are also installed at two ends of the measurement area for train identification and mapping of sensor measurement results. The interrogator and other measurement equipments are operated in the control center of the HTL depot.

4. Results and Discussions

Figure 4(a) shows the measured strain change of an FBG sensor when a typical 12-car passenger train passes a measurement point. The maximum strain change is ~250 $\mu\varepsilon$ (i.e., the wavelength change is ~0.25 nm). The 48 axles of the train are clearly indicated in the signal, as illustrated by the 48 peaks. The characteristics of strain change experienced by the rail induced by a passing train depend on the speed and weight of the train, as well as conditions of rail and wheels. The low-frequency component of the signal mainly comes from the axle load of the train as depicted by the strain peaks of Figure 4(a), those peaks also show the slightly heavy motor cars, and this signal is essential information for studying train axle counting system [13].

Figures 4(b) to 4(d) show the enlarged sections of Figure 4(a) that indicate the measured strain responses of the first to third cars of the train accordingly. Because these results are measured by the same sensor within a short period of time, they are therefore virtually collected under the same rail condition and reflected only the difference in the condition of the wheels. Obviously, Figure 4(b) shows a smooth strain signal generated by the first car while the signal generated by the third car as shown in Figure 4(d) is the noisiest among the three. Table 1 shows the wheel condition information of the three cars which is provided by the MTR, the OOR measurement in this table is conducted by using contact gauge in maintenance depot. The OOR of the wheels of the third car is much higher than those of the other two ones, and there is some thread wear in the wheels of the second car. In other words, the wheel condition of the first car is the best and that of the third car is the worst. Imperfect wheels of the third car exert periodic impact force onto the track and hence induce the measured uneven strain impulse as depicted by the noisy signal of Figure 4(d). Therefore smoother strain signal represents better condition of the wheels and this is consistent with the studies described previously [3, 6].

A condition index (CI) system has been developed to express the wheel condition quantitatively. This system processes the strain signal of the four wheels (left or right side) of a train car and generates a CI that essentially indicates the condition of the four wheels (if the condition of any wheel is not in good condition, the system can generate a CI to indicate the wheels of the train car need to be maintained, but cannot distinguish which wheel is not in good condition because the system processes the strain signal of the four wheels as a whole. The reason of processing four wheels as a whole is that railway operators normally do wheel reprofiling on a train car basis). The low-frequency component of the strain signal is first filtered out by using a low-pass filter with a cutoff frequency of 20 Hz, Figure 5(a) gives the low-pass filter result of the signal of Figure 4(d). This signal basically consists of the information of axle loading of the train induced by its weight. The train speed (v) can be deduced from the distance between two wheels and the time between the peaks of the signal. Figure 5(b) shows the high-pass-filtered signal which carries the wheel condition information, and the signal is then decomposed to different frequency components by fast Fourier transform (FFT), as shown in Figure 5(c). The distribution shows that the majority of the strain change is located in the frequency range of 20 to 200 Hz while others are mainly noise at the frequency above 200 Hz. Further experimental works has confirmed that higher strain change over this frequency range represents a worse wheel or rail conditions. Moreover, higher train speed (v) generates higher average strain change which increases 0.01 $\mu\varepsilon$ for a 1 km/h increment with the train speed running at 50 to 90 km/h. The equation for calculating

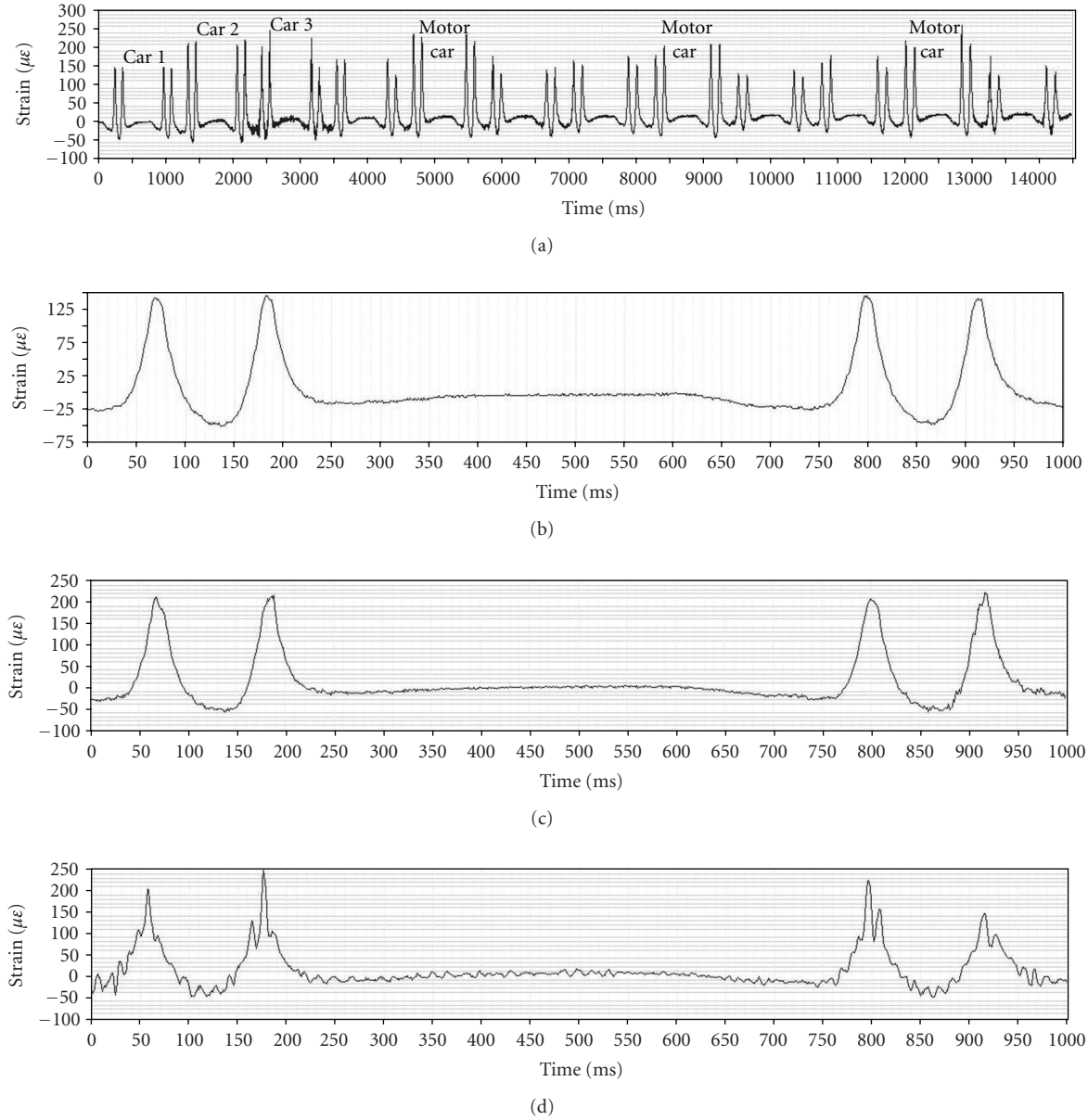

Figure 4: The measured strain change of (a) a 12-car passage train; (b) the first car; (c) the second car; (d) the third car.

Table 1: Wheel condition information of the three train cars.

Car number	OOR (on average)	Flat	cavity	Flange thin	Ellipse	Tread wear	Vibration
1	0.36	\	\	\	\	\	\
2	0.38	\	\	\	\	*	\
3	0.65	\	\	\	\	\	\

CI is therefore given by

$$\mathrm{CI} = \frac{\bar{\varepsilon}}{v} \times A, \tag{2}$$

where $\bar{\varepsilon}$ is the average value of the strain changes in the frequency range of 20 to 200 Hz, A is a scaling factor requires for matching the CI value within a range of 0 to 10.

The FBG monitoring system with CI was tested continuously over ten months, and the CIs of the twenty-nine passenger trains running in East Rail have been collected. Figures 6(a) and 6(b) show the evolutions of the CI over the 10-month test period of train cars 027_039 and 072_049, respectively, a single dot represents the train car passing

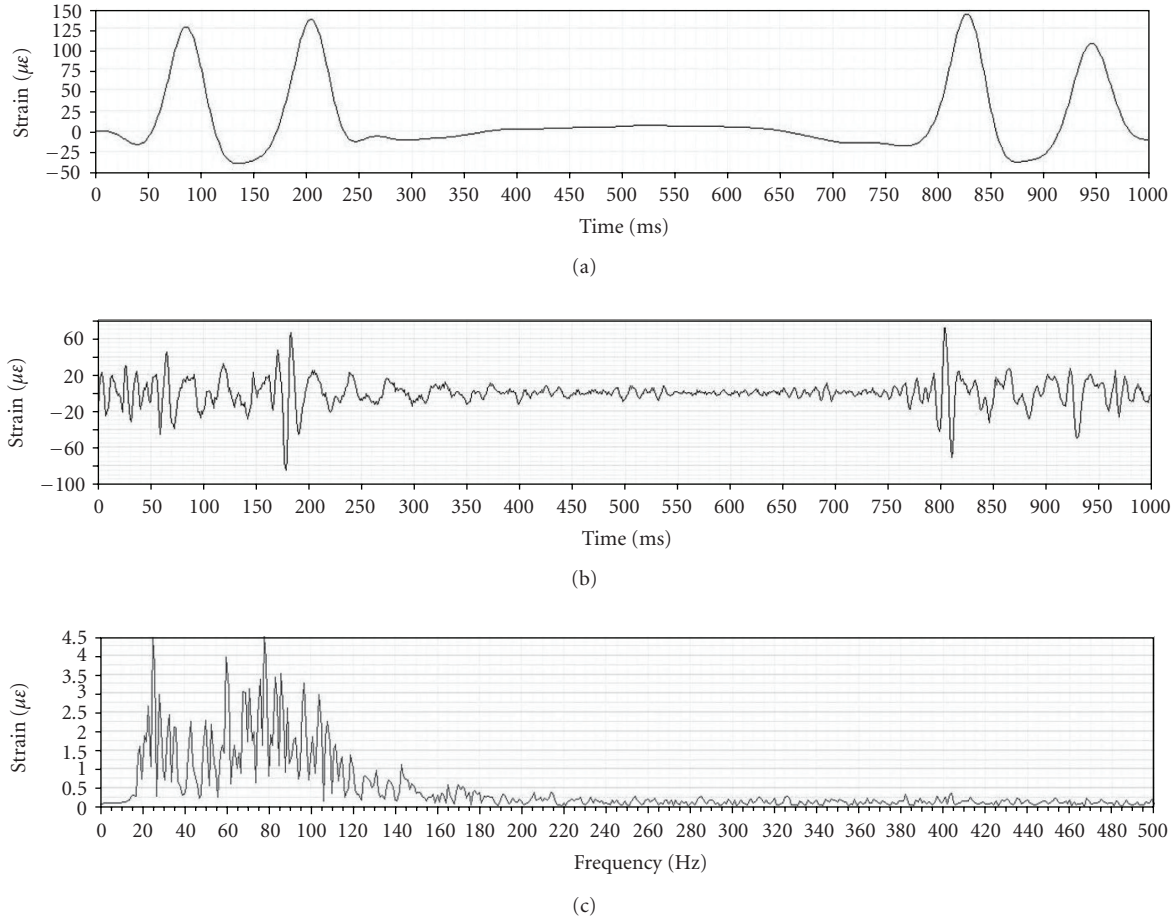

Figure 5: (a) The low-passed-filtered result of the signal in Figure 4(d); (b) the high-passed-filtered result of the signal in Figure 4(d); (c) frequency spectrum of the signal in (b) processed by FFT.

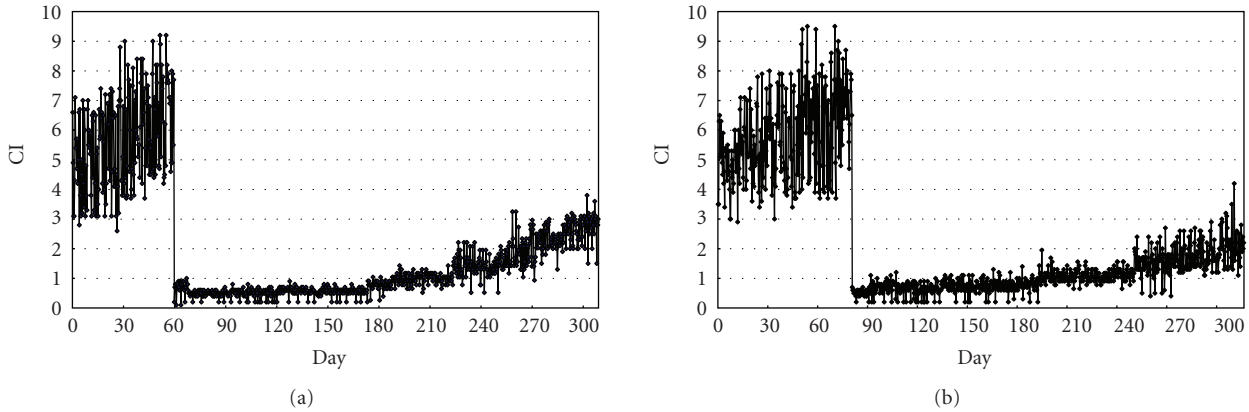

Figure 6: CI generated over ten months' period for (a) the left-side wheel of the train car 027_039; (b) the right-side wheel of the train car 072_049.

the measurement point once. It can be noted that the CI gradually increases for the first two/three months during the test until the wheels are reprofiled by depot grinding machine, the CI is substantially reduced from an average value of ∼7 to less than ∼1. After wheel reprofiling, the CI increases slightly and deteriorates again after ∼4 months in operation. This can be explained by the fact that newly turned wheels produce very little uneven strain on the rail and once a defect formed on a single wheel, deterioration of this wheel is accelerated and this also affects the other wheels

of the same bogie and hence degrades the overall wheel condition of the train car measured by the sensor system. It is also interesting to note from the figures that under normal train operation condition, the CI takes about 12 months to rise from ~1 of newly turned wheels to ~7 of just before wheels reprofiling, this time frame matches very well with the regular wheels reprofiling schedule exercised by the railway operator.

5. Conclusions

A real-time train wheel condition monitoring system using FBG sensors to measure the track strain response upon wheel-rail interaction is proposed and developed. The principle of FBG sensor and its optical characteristics are briefly reviewed, together with the description of the sensor packaging and field test. An algorithm to generate the CI value for indicating the train wheel condition is described, followed by the field test results and discussions.

The system has been proven to be able to continuously monitor the conditions of the wheel and identify wheel defects in time. The system has the advantage of providing real-time and in-service measurement of wheel condition. Moreover, FBG sensors used in this system are very low in optical loss and immunity from EMI is particular suitable for electrified railways with track spanning over tens or even hundreds of kilometers. Further test and verifications with wheel and rail condition data are still required to ensure the long-term reliability of the proposed system. To improve the measurement accuracy and overall integrity of the system, a more intelligent analysis technique based on the previous wheel and rail conditions information and the results of a measurement point with more FBG sensors installed is now under investigation. A more advanced FBG-based system which can differentiate the defects of wheel and rail, as well as their types and levels, is the next stage of the real-time railway condition monitoring development.

Acknowledgments

The authors would like to express their gratitude to financial support from Shantou University and the Hong Kong Polytechnic University, and the technical support from the Hong Kong MTR.

References

[1] J. C. O. Nielsen and A. Johansson, "Out-of-round railway wheels-a literature survey," *Proceedings of the Institution of Mechanical Engineers, Part F: Journal of Rail and Rapid Transit*, vol. 214, no. 2, pp. 79–91, 2000.

[2] F. Attivissimo, A. Danese, N. Giaquinto, and P. Sforza, "A railway measurement system to evaluate the wheel-rail interaction quality," *IEEE Transactions on Instrumentation and Measurement*, vol. 56, no. 5, pp. 1583–1589, 2007.

[3] A. Johansson and J. C. O. Nielsen, "Out-of-round railway wheels—wheel-rail contact forces and track response derived from field tests and numerical simulations," *Proceedings of the Institution of Mechanical Engineers, Part F: Journal of Rail and Rapid Transit*, vol. 217, no. 2, pp. 135–145, 2003.

[4] A. Johansson, "Out-of-round railway wheels-assessment of wheel tread irregularities in train traffic," *Journal of Sound and Vibration*, vol. 293, no. 3–5, pp. 795–806, 2006.

[5] M. Guagliano and M. Pau, "An experimental-numerical approach for the analysis of internally cracked railway wheels," *Wear*, vol. 265, no. 9-10, pp. 1387–1395, 2008.

[6] P. Remington and J. Webb, "Estimation of wheel/rail interaction forces in the contact area due to roughness," *Journal of Sound and Vibration*, vol. 193, no. 1, pp. 83–102, 1996.

[7] E. Matzan, "System for detection of defects in railroad car wheels," U.S. Patent 7213789, 2007.

[8] D. R. Anderson, "Detecting flat wheels with a fiber-optic sensor," in *Proceedings of the ASME/IEEE 2006 Joint Rail Conference (JRC '06)*, pp. 25–30, April 2006.

[9] H. Y. Tam, S. Y. Liu, B. O. Guan, W. H. Chung, T. H. T. Chan, and L. K. Cheng, "Fiber Bragg grating sensors for structural and railway applications," in *Advanced Sensor Systems and Applications II*, vol. 5634 of *Proceedings of SPIE*, Beijing, China, November 2004.

[10] K. Y. Lee, K. K. Lee, and S. L. Ho, "Exploration of using FBG sensor for derailment detector," *WSEAS Transactions Topics Systems*, vol. 3, pp. 2433–2439, 2004.

[11] K. Y. Lee, K. K. Lee, and S. L. Ho, "Exploration of using FBG sensor for axle counter in railway engineering," *WSEAS Transactions Topics Systems*, vol. 3, pp. 2440–2447, 2004.

[12] H. Y. Tam, S. Y. Liu, W. H. Chung, T. K. Ho, S. L. Ho, and K. K. Lee, "Smart railway sensor network using fiber Bragg grating sensors as sensing elements," in *Smart Materials and Smart Structures Technology*, vol. 1, pp. 159–169, Techno-Press, Daejeon, Korea, 2005.

[13] C. L. Wei, C. C. Lai, S. Y. Liu et al., "A fiber Bragg grating sensor system for train axle counting," *IEEE Sensors Journal*, vol. 10, no. 12, pp. 1905–1912, 2010.

[14] A. D. Kersey, M. A. Davis, H. J. Patrick et al., "Fiber grating sensors," *Journal of Lightwave Technology*, vol. 15, no. 8, pp. 1442–1462, 1997.

[15] T. H. T. Chan, L. Yu, H. Y. Tam et al., "Fiber Bragg grating sensors for structural health monitoring of Tsing Ma bridge: background and experimental observation," *Engineering Structures*, vol. 28, no. 5, pp. 648–659, 2006.

[16] E. J. Friebele, C. G. Askins, A. B. Bosse et al., "Optical fiber sensors for spacecraft applications," *Smart Materials and Structures*, vol. 8, no. 6, pp. 813–838, 1999.

[17] N. E. Fisher, J. Surowiec, D. J. Webb et al., "In-fibre Bragg gratings for ultrasonic medical applications," *Measurement Science and Technology*, vol. 8, no. 10, pp. 1050–1054, 1997.

[18] B. O. Guan, H. Y. Tam, and S. Y. Liu, "Temperature-independent fiber Bragg grating tilt sensor," *IEEE Photonics Technology Letters*, vol. 16, no. 1, pp. 224–226, 2004.

[19] Y. J. Rao, "Recent progress in applications of in-fibre Bragg grating sensors," *Optics and Lasers in Engineering*, vol. 31, no. 4, pp. 297–324, 1999.